

Green Chemistry

Accepted Manuscript



This article can be cited before page numbers have been issued, to do this please use: A. M. Bahmanpour, A. Hoadley and A. Tanksale, *Green Chem.*, 2015, DOI: 10.1039/C5GC00599J.



This is an *Accepted Manuscript*, which has been through the Royal Society of Chemistry peer review process and has been accepted for publication.

Accepted Manuscripts are published online shortly after acceptance, before technical editing, formatting and proof reading. Using this free service, authors can make their results available to the community, in citable form, before we publish the edited article. We will replace this *Accepted Manuscript* with the edited and formatted *Advance Article* as soon as it is available.

You can find more information about *Accepted Manuscripts* in the [Information for Authors](#).

Please note that technical editing may introduce minor changes to the text and/or graphics, which may alter content. The journal's standard [Terms & Conditions](#) and the [Ethical guidelines](#) still apply. In no event shall the Royal Society of Chemistry be held responsible for any errors or omissions in this *Accepted Manuscript* or any consequences arising from the use of any information it contains.

PAPER

Formaldehyde Production via Hydrogenation of Carbon Monoxide in Aqueous Phase

Cite this: DOI: 10.1039/x0xx00000x

Ali Mohammad Bahmanpour,^a Andrew Hoadley^a and Akshat Tanksale^{*a},Received 00th January 2012,
Accepted 00th January 2012

DOI: 10.1039/x0xx00000x

www.rsc.org/

Formaldehyde (HCHO) is an essential building block in many industries for producing value-added chemicals like resins, polymers and adhesives. Industrially formaldehyde is produced via partial oxidation and/or dehydrogenation of methanol. Methanol is produced from natural gas in a series of processes, with synthesis gas as an intermediate. This study presents for the first time formaldehyde production via hydrogenation of carbon monoxide in the aqueous phase, which eliminates the need for methanol synthesis, which may potentially save capital costs and reduce energy consumption. Gas phase hydrogenation of CO into formaldehyde is thermodynamically limited and therefore, resulted in low CO conversion of only 1.02×10^{-4} %. However, the aqueous phase hydrogenation of CO into formaldehyde was found to be thermodynamically favourable and kinetically limited. Highest CO conversion of 19.14% and selectivity of 100% was achieved by using Ru-Ni/Al₂O₃ catalyst at 353 K and 100 bar. The rapid hydration of formaldehyde in the aqueous phase to form methylene glycol shifts the CO hydrogenation reaction equilibrium towards formaldehyde formation. Increasing the pressure and stirring speed increased the yield of formaldehyde, whereas increasing the temperature above 353 K resulted in a lower yield.

Introduction

Industrially, formaldehyde (HCHO) is produced in three stages – (a) Steam reforming of natural gas to produce syngas (Table 1, Eq.1), (b) Methanol (CH₃OH) Synthesis (Eq. 2) and (c) partial oxidation of CH₃OH to produce HCHO (Eq. 3). Alternatively, HCHO is industrially produced via dehydrogenation of CH₃OH (Eq. 4).^{1, 2} However, these are all high temperature reactions which require combustion, compression and large process units for purification, which are the root cause of energy losses.^{3, 4} We have recently shown that this series of processes from natural gas to HCHO production suffers from ~57% losses in exergy (i.e. energy quality).⁵ Given the large quantity of HCHO produced in the world, when combined with the high losses in exergy, leads to high energy losses and also high CO₂ emissions, globally. Many researchers have tried to overcome this issue by finding ways to produce HCHO directly from natural gas by partial oxidation of CH₄ (Eq. 5).⁶⁻⁸ However, there has been no significant progress to date due to low CH₄ conversion and poor selectivity.⁶ The rate of HCHO decomposition into CO and H₂ is much greater than the rate of partial oxidation of CH₄, especially at temperatures in excess of 373 K, which means that in order to produce HCHO selectively, one must limit the conversion of CH₄ in

Eq. 5 to a very small value. Moreover, if we consider that natural gas is a valuable energy resource, it becomes evident that an alternative feedstock for HCHO production is much needed. An alternative is direct conversion of synthesis gas into HCHO. Syngas can be produced from a range of sources including biomass and allows the mole fractions of CO to H₂ to be controlled more easily through the use of H₂O and CO₂ which is helpful in climate change abatement.⁹ Gas phase hydrogenation of CO to produce HCHO (Equation 6) is not feasible because of positive Gibbs free energy change of the reaction.¹⁰ Only trace amount of HCHO in the product has been reported with the highest CO conversion of 0.2%.¹¹ Therefore, direct conversion of synthesis gas into HCHO has not been studied extensively. In this report, hydrogenation of CO into HCHO in a slurry reactor is presented as a viable alternative. By comparing with gas phase conversion in a fixed bed reactor, it is demonstrated that the thermodynamic limitation can be overcome in the slurry reactor. A low temperature active catalyst is desirable for the slurry phase reaction as the reaction was found to be favourable below 373 K. Generally, Ni Pd and Ru are considered as active hydrogenation catalysts in the literature for many reactions.¹²⁻²¹ Based on the density functional theory (DFT) studies done in the literature, Pd and Ni have been shown to produce HCHO as an intermediate of CO hydrogenation to produce CH₃OH.^{22, 23} Previous studies have also shown that bi-metallic Pd-Ni catalyst has better reducibility and higher metal surface area.²⁴ Therefore, Pd-Ni and Ru-Ni supported on γ -Al₂O₃ were used as the catalysts in this study.

^a Catalysis for Green Chemicals Group
Department of Chemical Engineering
Monash University, Clayton, VIC 3800, Australia
* Email: akshat.tanksale@monash.edu
Ph.: 61 3 99024388 and Fax : 61 3 99055686

Table 1 Chemical reactions used for the production of HCHO in the gas phase

Reaction Name	Reaction Stoichiometry	Equation No.
Steam Reforming	$CH_4 + H_2O \rightleftharpoons CO + 3H_2$	$\Delta\hat{H}_r^\circ = +206 \text{ kJ.mol}^{-1}$ (1)
Methanol Synthesis	$CO + 2H_2 \rightleftharpoons CH_3OH$	$\Delta\hat{H}_r^\circ = -91 \text{ kJ.mol}^{-1}$ (2)
Methanol Partial Oxidation	$CH_3OH + \frac{1}{2}O_2 \rightarrow HCHO + H_2O$	$\Delta\hat{H}_r^\circ = -159 \text{ kJ.mol}^{-1}$ (3)
Methanol Dehydrogenation	$CH_3OH \rightleftharpoons HCHO + H_2$	$\Delta\hat{H}_r^\circ = +84 \text{ kJ.mol}^{-1}$ (4)
Methane Partial Oxidation	$CH_4 + O_2 \rightarrow HCHO + H_2O$	$\Delta\hat{H}_r^\circ = -319 \text{ kJ.mol}^{-1}$ (5)
Syngas to Formaldehyde in Gas Phase	$CO + H_2 \rightleftharpoons HCHO$	$\Delta\hat{H}_r^\circ = -5.4 \text{ kJ.mol}^{-1}$, $\Delta G^\circ = +34.6 \text{ kJ.mol}^{-1}$ (6)

Results and Discussion

Catalyst Characterization

BET surface area of the support and CO-chemisorption results are shown in Table 2. BET surface area is given for the commercial γ - Al_2O_3 before metal impregnation. It is expected that the surface area reduced to some extent after impregnation.²⁴

The nominal and actual metal content of the catalysts are presented in Table 2, which shows good agreement. The promoter content was calculated based on the mass balance as the actual content of the NiO and Al_2O_3 was measured by X-ray Fluorescence (XRF) spectroscopy. Based on the amount of CO adsorption on the catalyst surface, metal dispersion was calculated according to the following formula:

$$Dispersion(\%) = \frac{M_{CO} \times AW}{WF} \times 100 \quad (7)$$

where M_{CO} is the amount of adsorbed CO ($\mu\text{mol.g}^{-1}$), AW is the atomic weight of the metals ($\text{g.}\mu\text{mol}^{-1}$), and WF is the weight fraction of the metals in the catalysts. Table 2 shows that CO uptake and metal dispersion of Ru-Ni/ Al_2O_3 was significantly higher than Pd-Ni/ Al_2O_3 , even though similar metal loading was used. This suggests that the supported Ru-Ni nanoparticles are much smaller than the Pd-Ni nanoparticles. This is confirmed from the Transmission Electron Microscopy (TEM) results shown in Figure 1. The nanoparticles sizes were estimated using ImageJ software (NIH) and shown in the in-set. The mean particle size of Pd-Ni nanoparticles was 3.69 nm compared to the mean particle size of Ru-Ni nanoparticles of 2.14 nm. Lower particle size and hence higher dispersion of the catalyst nanoparticles is favourable for HCHO formation because it would provide higher surface area for CO and H_2 adsorption which is expected to be a necessary step for hydrogenation reaction.

The X-ray Diffraction (XRD) patterns of the calcined and reduced Ru-Ni/ Al_2O_3 and Pd-Ni/ Al_2O_3 catalysts are presented in Figure 2. The peaks representing PdO (34.06°) and RuO_2 (28.19° and 34.06°) disappeared after reduction and peaks representing Pd^0 (40.15°) and Ru^0 (43.98°) were observed, which confirmed complete reduction of the catalysts.^{25, 26} Broad NiO and Ni^0 peaks were also observed at 62.88° and 51.83° 2θ angles, which also confirm that the Ni nanoparticles are finely dispersed.²⁷

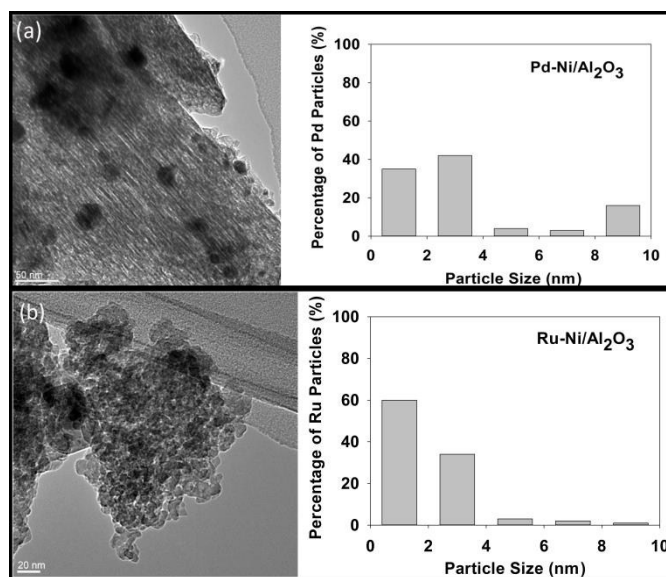


Figure 1 TEM image and particle size distribution of a) Pd-Ni/ Al_2O_3 . Scale bar= 50nm and b) Ru-Ni/ Al_2O_3 . Scale bar= 20nm

Thermodynamic Investigation

Hydrogenation of CO into HCHO in the gas phase and aqueous phase was thermodynamically investigated using the HSC Chemistry® version 7.11 (Outotec, Finland) software and published data²⁸ for a wide range of temperatures (298-623 K) and pressures (50-500 bar). The results (Table 3) show that the Gibbs free energy (ΔG) of the reaction is positive in the gas phase and it increases with increasing temperature. Therefore the reaction is non-spontaneous at all temperatures above 298 K. The equilibrium constant of the gas phase reaction is very low ($8.76 \times 10^{-7} \text{ mol}^{-1}$ at 298 K) which, along with the positive ΔG , suggests that the forward reaction is not favourable. In the aqueous phase however, ΔG of the reaction is negative at low temperatures and the equilibrium constant is relatively high (17.33 mol^{-1} at 298 K), which suggests that HCHO formation is favourable in the aqueous phase. This is because the heat of solution of HCHO is -62 kJ.mol^{-1} ,¹ which is also relatively high while the heat of solution of H_2 and CO is

Table 2: BET surface area, metal loading, and CO chemisorption data

Catalyst	Nominal Metal Loading (%w/w)	Actual Metal Loading* (%w/w)	Total CO uptake ($\mu\text{mol.g}^{-1}$)	Metal Dispersion (%)	BET Surface area of the Support ($\text{m}^2.\text{g}^{-1}$)
Ru-Ni/ Al_2O_3	Ni-10	Ni-9.3	41.96	2.33	108.51
	Ru-1	Ru-1.4			
Pd-Ni/ Al_2O_3	Ni-10	Ni-9.5	26.50	1.47	
	Pd-1	Pd-1.3			

insignificant in comparison. This results in the improvement of the equilibrium conversion. The effect of pressure on the Gibbs free energy of the reaction in the aqueous phase is shown in Figure 3. The data presented in this Figure are calculated based on the interpolation of experimental data presented by Oelkers et al.²⁸ It can be seen that as the operating pressure increases, the Gibbs free energy of the reaction decreases. Although it is concluded that higher pressures are favourable for this reaction, the operating pressure in this study was limited to 100 bar by the maximum available gas cylinder pressure.

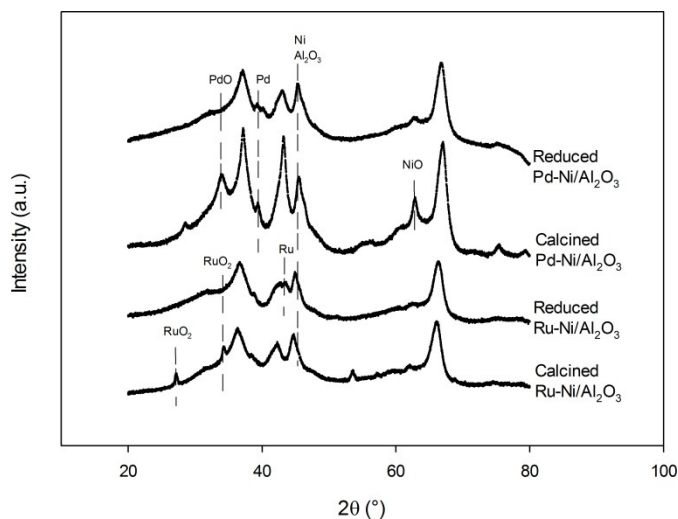


Figure 2 XRD patterns of calcined and reduced Pd-Ni/ Al_2O_3 and Ru-Ni/ Al_2O_3

It can be seen in Table 3, the equilibrium conversion of the reaction is significantly higher in the aqueous phase, which is due to low ΔG of the components in the aqueous media. Therefore, the reaction is thermodynamically feasible in the liquid phase and can achieve sufficiently high equilibrium conversion to make this process viable. The reaction is therefore expected to be kinetically limited, which can be improved by the use of an appropriate catalyst.

Comparison of HCHO Production in Fixed Bed and Slurry Reactors

Fixed Bed Reactor

Figure 4 shows the effect of pressure (Figure 4a) and temperature (Figure 4b) on the molar yield of HCHO using Pd-Ni/ Al_2O_3 as the catalyst in the gas phase reaction.

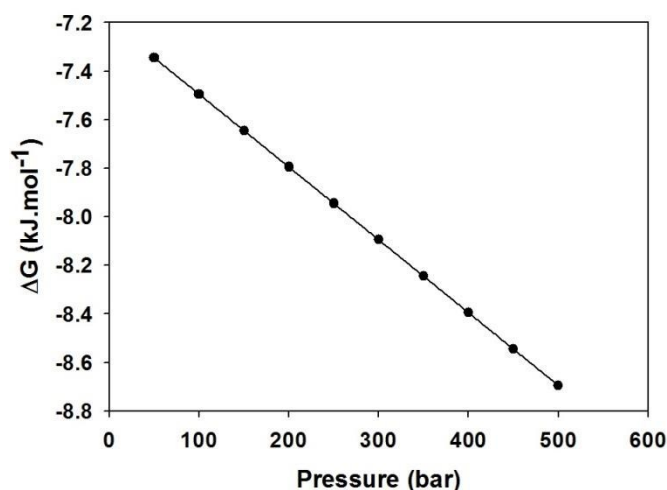


Figure 3 Effect of pressure on the Gibbs free energy of the reaction in the aqueous phase, $T = 298 \text{ K}$ ²⁸

As two moles of reactants are combining to form one mole of the product, higher pressures favour the forward reaction, according to Le Chatelier's Principle and the previous studies.^{2, 10} The highest yield of HCHO ($8.2 \times 10^{-3} \text{ mmol.L}^{-1}.\text{g}_{\text{cat}}^{-1}$) in fixed bed gas phase reactor was obtained at 117 bar pressure at 293 K, which equates to conversion of only $1.02 \times 10^{-4} \%$, which is well below the equilibrium conversion. It was also confirmed from the experiments, as shown in Figure 4b, higher temperatures are unfavourable for the reaction in the gas phase because the overall yield of HCHO reduced from $4.84 \times 10^{-3} \text{ mmol.L}^{-1}.\text{g}_{\text{cat}}^{-1}$ to less than $2.12 \times 10^{-3} \text{ mmol.L}^{-1}.\text{g}_{\text{cat}}^{-1}$ after 180 min reaction time.

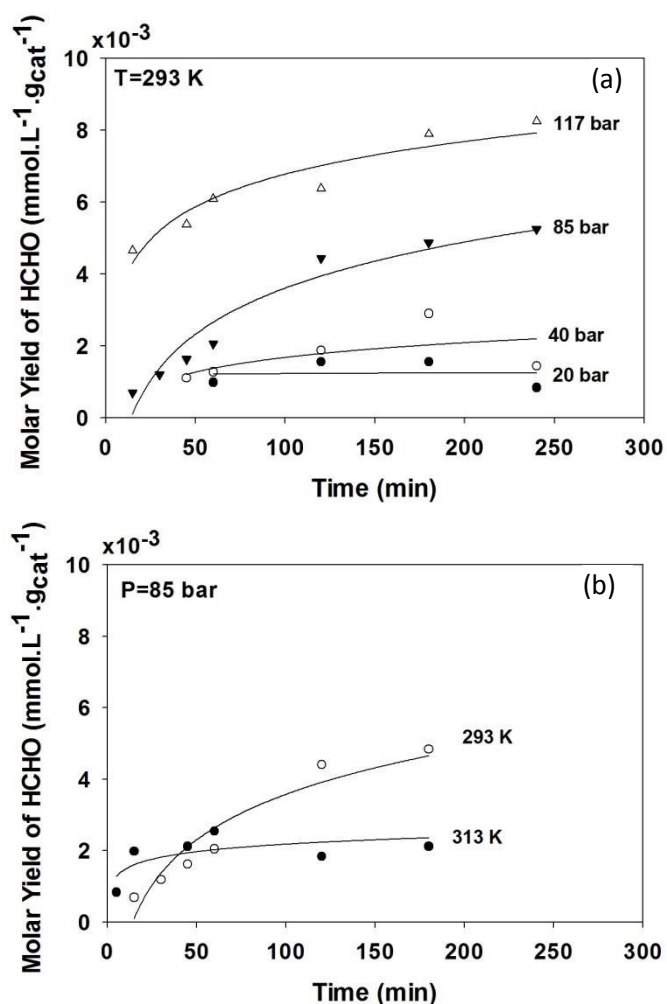
Slurry Reactor

Figure 5 presents the Arrhenius plot of the reaction in the aqueous phase after the first two hours of operation. The highest rate of reaction in the first two hours was $0.0378 \mu\text{mol.L}^{-1}.\text{s}^{-1}$ at 403 K. The activation energy was calculated to be $27.58 \text{ kJ.mol}^{-1}$ for the Ru-Ni/ Al_2O_3 as the catalyst. Figure 6 and Figure 7 show the effect of temperature on the yield of HCHO as a function of time. Although the equilibrium constant decreased with increasing temperature in the aqueous phase, HCHO production rate increased which proves that the process was kinetically limited, unlike the gas phase which was thermodynamically limited. After 48 hours, it was observed that HCHO yield was higher at 353 K and 373 K compared to 403 K.

As shown in Figure 7, the highest level of the HCHO yield was $4.55 \text{ mmol.L}^{-1}.\text{g}_{\text{cat}}^{-1}$ at 72 hours of operation at 353 K, which is

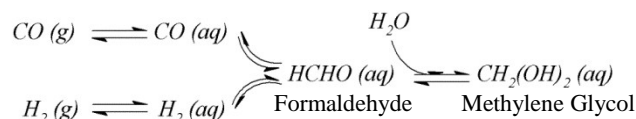
Table 3 CO hydrogenation thermodynamic data

Gas Phase				Aqueous Phase		
T	X_e	ΔG	K	X_e	ΔG	K
K	%	kJ.mol ⁻¹	mol ⁻¹	%	kJ.mol ⁻¹	mol ⁻¹
298	4.38×10 ⁻³	34.565	8.760×10 ⁻⁷	31.40	-7.071	17.332
323	4.67×10 ⁻³	37.297	9.348×10 ⁻⁷	18.42	-5.648	8.186
373	4.88×10 ⁻³	42.933	9.764×10 ⁻⁷	3.86	-1.297	1.519
423	4.86×10 ⁻³	48.705	9.711×10 ⁻⁷	5.84×10 ⁻¹	4.853	2.52×10 ⁻¹
473	4.70×10 ⁻³	54.586	9.405×10 ⁻⁷	8.88×10 ⁻²	12.343	4.30×10 ⁻²
523	4.49×10 ⁻³	60.554	8.983×10 ⁻⁷	1.50×10 ⁻²	21.129	8.00×10 ⁻³
573	4.26×10 ⁻³	66.592	8.523×10 ⁻⁷	1.72×10 ⁻³	31.171	1.00×10 ⁻³
623	4.03×10 ⁻³	72.685	8.068×10 ⁻⁷	3.95×10 ⁻⁴	43.053	2.46×10 ⁻⁴

Figure 4: Effect of (a) pressure and (b) temperature on the molar yield of HCHO in the fixed bed reactor using Pd-Ni/Al₂O₃

equal to turn over frequency (TOF) of 0.0602 h⁻¹. The highest conversion of soluble CO was 19.14% which is significantly higher than the published works on gas phase CO

hydrogenation.^{10, 11} This conversion is also higher than the theoretical equilibrium conversion because the equilibrium is shifted when HCHO is dissolved in water. HCHO reacts with water rapidly to form methylene glycol (CH₂(OH)₂).²⁹ In the solution, HCHO and CH₂(OH)₂ co-exists in dynamic equilibrium with a HCHO/CH₂(OH)₂ ratio of 1:2499 at STP and pH = 7,³⁰ which means 99.96% of HCHO is converted to CH₂(OH)₂. Therefore, HCHO produced in this method is instantly absorbed in water, shifting the reaction equilibrium in the forward direction, as shown below.



Conversion of HCHO into CH₂(OH)₂ has been well studied in the literature.^{29, 31-35} CH₂(OH)₂ also polymerizes to form polyoxymethylene ((CH₂O)_n).³³ However, the polymerization reaction rate is much lower compared with the rate of hydration and dehydration reactions and it can be inhibited by CH₃OH.²⁹ Based on the studies done by Whinkelman et al, the HCHO hydration rate (k_h) and the equilibrium constant for hydration (K_h) are calculated to be as follows:^{34, 35}

$$k_h = 2.04 \times 10^5 \times e^{\frac{-2936}{T}} \quad (8)$$

$$K_h = e^{\frac{3769}{T} - 5.494} \quad (9)$$

It is demonstrated in Figure 7 that the HCHO yield peaked in all cases, and that peak shifted towards lower time as the temperature was increased. Therefore, higher temperatures promoted the side reaction in which HCHO (and CH₂(OH)₂) is consumed. The final product was checked for the presence of other possible compounds such as ethylene glycol. No other compound was detected in the liquid phase which indicates loss of HCHO into the gas phase.

Journal Name

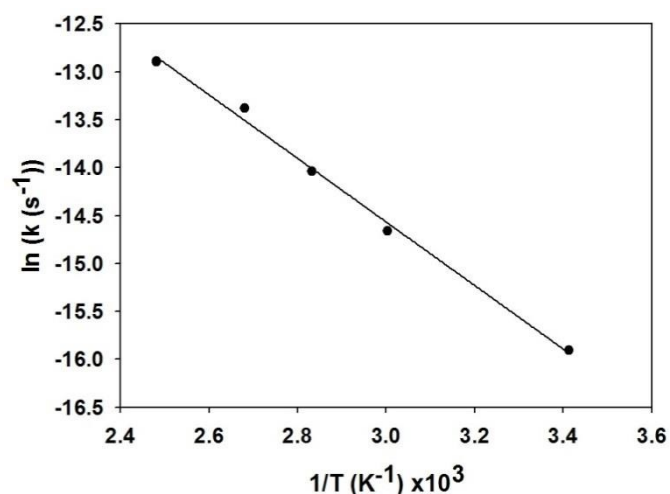


Figure 5: Reaction constant based on the first 2 hour of the reaction, P=100 bar, Catalyst: Ru-Ni/Al₂O₃

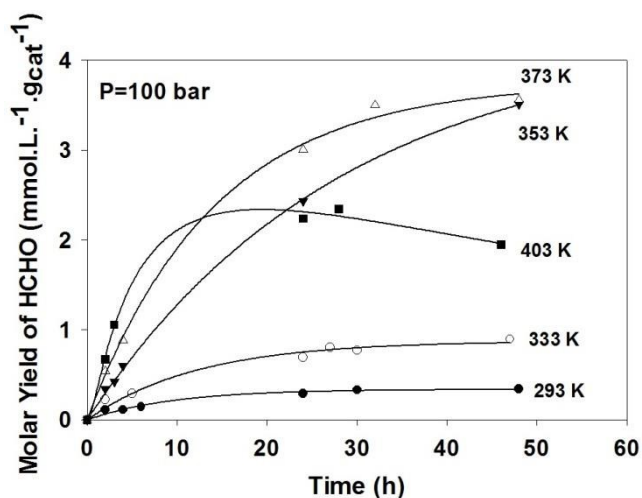


Figure 6: Effect of temperature on the molar yield of HCHO in the slurry reactor after 48 hours using Ru-Ni/Al₂O₃

At high temperatures and low pH values, the HCHO/CH₂(OH)₂ equilibrium shifts towards HCHO which may vaporise into the gas phase.²⁹ CH₂(OH)₂ is known to be very unstable in the gas phase because it tends to dehydrate rapidly to HCHO and water.³⁶ Therefore, heating a solution of HCHO and CH₂(OH)₂ may lead to HCHO emission.²⁹

Comparison of the HCHO yield in the fixed bed reactor and the slurry reactor at identical operating conditions are presented in Figure 8. The yield of HCHO in the slurry reactor at room temperature was more than an order of magnitude higher compared to the fixed bed reactor. The TOF of HCHO production was higher for the Ru-Ni/Al₂O₃ than Pd-Ni/Al₂O₃ catalyst in the slurry reactor, which suggests that the former catalyst is more active in the aqueous conditions.³⁷ At room temperature in the aqueous phase, TOF for Ru-Ni/Al₂O₃ was 0.0475 h⁻¹ compared to 0.0319 h⁻¹ for Pd-Ni/Al₂O₃.

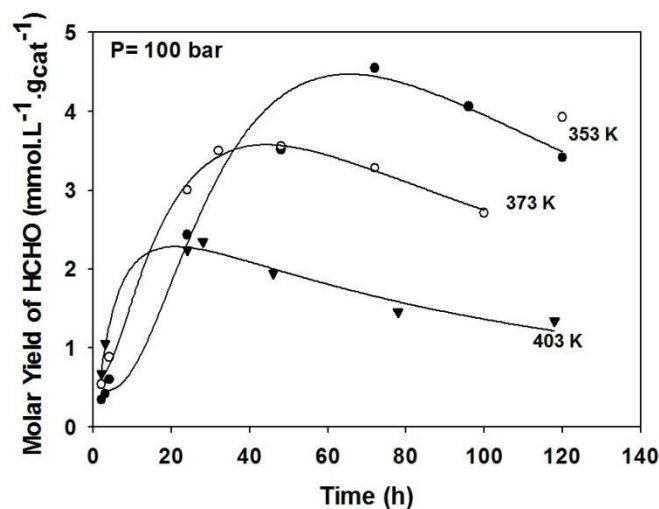


Figure 7: Effect of temperature on molar yield of HCHO in the slurry reactor after 120 hours using Ru-Ni/Al₂O₃

Effect of the Stirring Speed on the Aqueous Phase Process

Effect of stirring speed was tested by varying RPM= 0, 400, 800, 1200 at 298 K at 100 bar using Ru-Ni/Al₂O₃. Figure 9 shows that the yield of HCHO increased from 0.26 mmol.L⁻¹.gcat⁻¹ to 0.4 mmol.L⁻¹.gcat⁻¹ as the stirring rate increased from 0 RPM to 800 RPM. But further increasing the RPM did not increase the yield of HCHO. There are many factors which affects catalytic conversion in a slurry reaction. In a non-stirred reactor the catalyst particles may settle at the bottom of the reactor which makes the process diffusion limited. Stirring can decrease the mass transfer limitation by increasing the convective mass transfer coefficient and exposing the catalyst surface to the dissolved gases. Increasing the mass transfer coefficient increases the apparent global rate of reaction and this was observed in Figure 9. However, once the rate of mass transfer is sufficiently high, further increasing the stirring rate has no impact on the global rate of reaction because the reaction is kinetically controlled.^{38, 39} Therefore it can be concluded that at 800 RPM the test was conducted in a kinetically controlled regime.

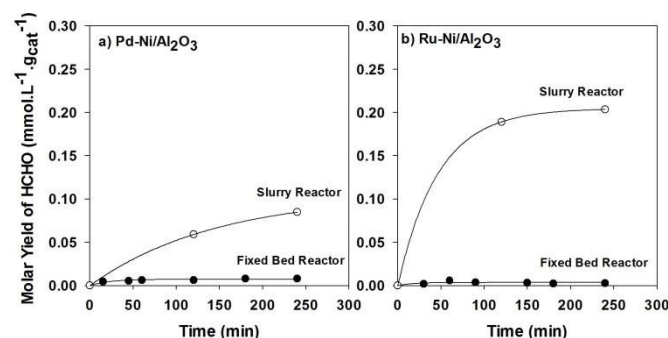


Figure 8: Comparison between the results of the fixed bed reactor and the slurry reactor at 293 K and 100 bar for a) Pd-Ni/Al₂O₃ and b) Ru-Ni/Al₂O₃

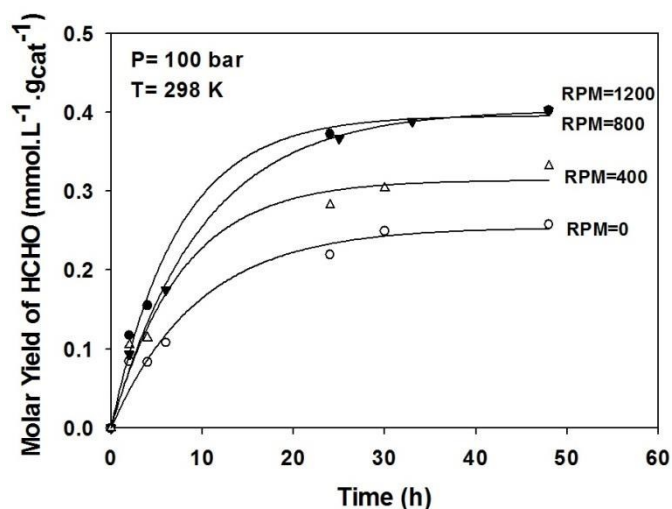


Figure 9: Effect of the stirrer rotation speed on the molar yield of HCHO using Ru-Ni/Al₂O₃

Experiments and Methods

Catalyst Preparation and Characterization

The catalysts used in this process were produced by the wet impregnation method followed by calcination. Nickel nitrate ((NO₃)₂.6H₂O, Sigma-Aldrich), ruthenium chloride (RuCl₃.xH₂O, Sigma-Aldrich) and palladium nitrate (10 wt% Pd(NO₃)₂ in 10wt% nitric acid, Sigma-Aldrich) were used as Ni, Ru and Pd precursors, respectively. The desirable amounts of Ni and noble metal precursors were added simultaneously to commercial γ -Al₂O₃ suspended in 20 ml water. The mixture was stirred at 333 K for 6 h. The suspension was then dried at 373 K overnight. The dried catalyst was calcined at 873 K for 6 h.

Fixed bed reactor tests were started by reducing the catalyst *in-situ* prior to the experiment by flowing 50 ml.min⁻¹ of H₂ through the catalyst bed at 673 K for 5 h followed by purging with Ar at 673 K for 1 h. The catalyst bed was cooled to room temperature under Ar flow overnight. For the slurry reactor tests, the same procedure of catalyst reduction was carried out *ex-situ*.

BET surface area of the support was measured by the N₂ physisorption method in Micrometric ASAP2020 at 77 K. CO chemisorption was used to measure the amount of active sites of each catalyst and the metal dispersion percentage using ASAP2020 (Micrometrics). XRF was used to determine the actual mass percentage of the metals using an Ametek Spectro iQ II XRF. XRD patterns of fresh calcined and reduced catalysts were recorded using a REGAKU MiniFlex 600 X-ray diffraction instrument equipped with a Ni-filtered Cu K α radiation in order to study the situation of the catalyst before and after reduction. XRD patterns were gained for 2 θ between 20° to 80° using step size of 0.01. TEM was used to evaluate the particle size of each promoter (Pd and Ru) in the fresh calcined catalysts and ImageJ 1.48 (National Institutes of Health) was used to generate the particle size distribution.

Fixed Bed Reactor

A schematic diagram of the fixed bed reactor setup is illustrated in Figure 10. CO and H₂ gases were mixed in 1:1 mole ratio (30 ml.min⁻¹ each) using mass flow controllers in a gas manifold prior to feeding it in the fixed bed reactor. The reactor was Swagelok 1/4" OD seamless tube in which 1 g of catalyst was fixed using quartz wool. The reactor was heated by a tube furnace which was used for *in-situ* reduction of the catalyst prior to the test. A back pressure regulator controlled the desired pressure upstream in the system. The gas stream leaving the back pressure regulator was passed through a scrubber containing 40 ml of 5 vol% CH₃OH in water to recover HCHO. CH₃OH was used in order to prevent hydrated HCHO molecules from polymerization. These runs were conducted at a range of pressures (20bar, 40bar, 85bar, and 117bar) and temperatures (293 K and 313 K). At the end of the run, the HCHO concentration was measured using the photometric cell test kit (Merck Millipore) in a DR 5000TM UV/VIS spectrophotometer (HACH Company, USA) at 575nm wavelength using a chromotropic acid method.⁴⁰ In this method, 4.5 ml of 75% sulphuric acid (H₂SO₄) was measured in a plastic tube. 0.1 g of chromotropic acid disodium salt dihydrate (C₁₀H₁₀Na₂O₁₀S₂) was added to the tube and was shaken vigorously. 3 ml of the sample (diluted if required) was added to the mixture. The intensity of the violet colour resulting from the reaction was checked in the spectrophotometer and quantified based on the pre-prepared calibration curve.

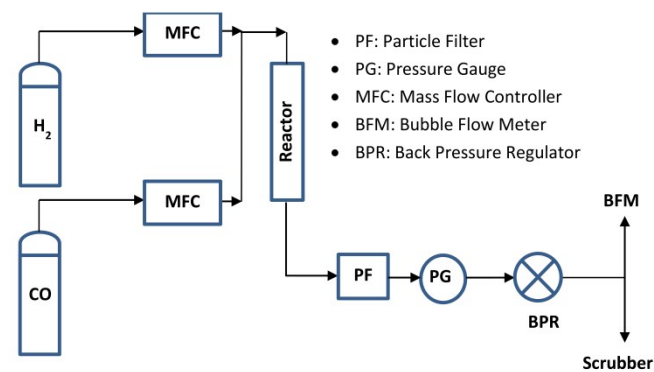


Figure 10: Schematic diagram of the fixed bed reactor setup

Slurry Reactor

The slurry reactor, illustrated in Figure 11, was charged with 40 ml of 5 vol% CH₃OH in water. 1 g of the desired catalyst was reduced *ex-situ* before adding it to the reactor. The reactor was subsequently pressurized up to the desired pressure with equimolar mixture of CO and H₂. Subsequently the reactor was heated to the desired temperature (293 K, 333 K, 353 K, 373 K, or 403 K). During the run, liquid samples were collected at regular intervals through the dip tube. HCHO concentration in the liquid samples was measured using a photometric cell test kit (Merck Millipore) in a DR 5000TM UV/VIS spectrophotometer (HACH Company, USA) at 575nm wavelength. Alternatively, the concentration was measured using a FluoroQuik fluorimeter version 4.3.A using 360nm/490nm as the excitation/emission wavelengths. In this method, a working reagent was prepared by addition of acetoacetanilide (C₁₀H₁₁NO₂) solution and ammonium acetate (C₂H₃O₂NH₄) solution (Amisience Corporation), as described elsewhere.⁴¹ 50 μ l of the working reagent was mixed with 50 μ l

of each sample and the mixtures were incubated in dark for 30 min before measuring the fluorescence intensity. The HCHO concentration was quantified based on the calibration curve provided.

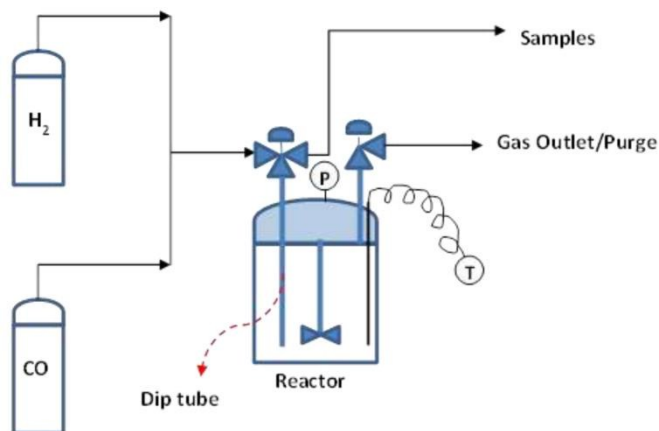


Figure 11: Schematic diagram of the slurry reactor setup

Conclusions

In this study, the direct formaldehyde (HCHO) production from synthesis gas in a slurry reactor is reported for the first time. Thermodynamic investigation showed that CO hydrogenation in the gas phase is limited by positive Gibbs free energy (ΔG) at all temperatures above 298 K, whereas in the aqueous phase the reaction is thermodynamically favourable because the ΔG is negative below 383 K. This resulted in low yield of HCHO in the fixed bed reactor, and significantly higher yield in the slurry reactor (8.25×10^{-3} and 8.48×10^{-2} mmol.L⁻¹.g_{cat}⁻¹, respectively, at 298 K in 4 h using Pd-Ni/Al₂O₃). The HCHO yield reduced with temperature in the fixed bed reactor, where the yield significantly increased with temperature in the slurry reactor. The highest yield of the HCHO was 4.55 mmol.L⁻¹.g_{cat}⁻¹ at 353 K after 72 h, which equates to conversion of 19.14% of soluble CO. This conversion is higher than the equilibrium conversion at this temperature because HCHO produced in the aqueous phase is rapidly absorbed by water and hydrated to produce methylene glycol which shifts the equilibrium of CO hydrogenation reaction towards formaldehyde production. The slurry phase method presented here may be a viable alternative for HCHO production which bypasses the methanol synthesis route. Since only water and small amount of methanol was used as solvent in a low temperature reaction, this method is greener than the current HCHO production methods. Synthesis gas and methanol may both be produced from biomass conversion technologies, which will offer environmentally friendly route for HCHO production. Currently, low solubility of CO and H₂ in water is one of limitations of this method; however, solubility of these reactants may be improved with the use of other solvents in future studies.

Notes and references

1. G. Reuss, W. Disteldorf, A. O. Gamer and A. Hilt, *Ullmann's Encyclopedia of Industrial Chemistry*, Wiley, Weinheim, 2003.
2. J. F. Walker, *Formaldehyde*, Reinhold Publishing Corporation, New York, 1967.

3. Q. Li, X. Wu, L. Ma and S. Hu, *Natural Gas Industry*, 2014, **34**, 144-151.
4. M. A. Rosen and D. S. Scott, *Int. J. Hydrogen Energy*, 1988, **13**, 617-623.
5. A. M. Bahmanpour, A. Hoadley and A. Tanksale, *Rev. Chem. Eng.*, 2014, **30**, 583-604.
6. S. B. Dake and R. V. Chaudhari, *J Chem Eng Data*, 1985, **30**, 400-403.
7. Purwanto, R. M. Deshpande, R. V. Chaudhari and H. Delmas, *J Chem Eng Data*, 1996, **41**, 1414-1417.
8. E. W. Blair and T. S. Wheeler, *The Analyst*, 1923, **48**, 110-112.
9. F. L. Chan and A. Tanksale, *ChemCatChem*, 2014.
10. R. H. Newton and B. F. Dodge, *Journal of American Chemical Society*, 1933, **55**.
11. G. T. Morgan, D. V. N. Hardy and R. A. Proctor, *J. Soc. Chem. Ind., London*, 1932, **51**, 1-7T.
12. K. Abdur-Rashid, S. E. Clapham, A. Hadzovic, J. N. Harvey, A. J. Lough and R. H. Morris, *J. Am. Chem. Soc.*, 2002, **124**, 15104-15118.
13. M. Araki and V. Ponc, *J. Catal.*, 1976, **44**, 439-448.
14. A. N. Fatsikostas and X. E. Verykios, *J. Catal.*, 2004, **225**, 439-452.
15. D. W. Goodman, R. D. Kelley, T. E. Madey and J. T. Yates Jr, *J. Catal.*, 1980, **63**, 226-234.
16. S. Hashiguchi, A. Fujii, J. Takehara, T. Ikariya and R. Noyori, *J. Am. Chem. Soc.*, 1995, **117**, 7562-7563.
17. P. G. Jessop, T. Ikariya and R. Noyori, *Nature*, 1994, **368**, 231-233.
18. S. Kidambi, J. Dai, J. Li and M. L. Bruening, *J. Am. Chem. Soc.*, 2004, **126**, 2658-2659.
19. V. C. H. Kroll, H. M. Swaan and C. Mirodatos, *J. Catal.*, 1996, **161**, 409-422.
20. Y. Niu, L. K. Yeung and R. M. Crooks, *J. Am. Chem. Soc.*, 2001, **123**, 6840-6846.
21. R. Noyori and S. Hashiguchi, *Acc. Chem. Res.*, 1997, **30**, 97-102.
22. M. Neurock, *Top. Catal.*, 1999, **9**, 135-152.
23. I. N. Remediakis, F. Abild-Pedersen and J. K. Nørskov, *J. Phys. Chem. B*, 2004, **108**, 14535-14540.
24. A. Tanksale, J. N. Beltramini, J. A. Dumesic and G. Q. Lu, *J. Catal.*, 2008, **258**, 366-377.
25. W. A. W. Abu Bakar, R. Ali and S. Toemen, *Scientia Iranica*, 2012, **19**, 525-534.
26. R. Wojcieszak, M. J. Genet, P. Eloy, P. Ruiz and E. M. Gaigneaux, *Journal of Physical Chemistry C*, 2010, **114**, 16677-16684.
27. J. Hanson and P. Norby, in *In-situ Characterization of Heterogeneous Catalysts*, John Wiley & Sons, Inc., 2013, pp. 121-146.
28. E. H. Oelkers, H. C. Helgeson, E. L. Shock, D. A. Sverjensky, J. W. Johnson and V. A. Pokrovskii, *J. Phys. Chem. Ref. Data*, 1995, **24**, 160.
29. I. J. Boyer, B. Heldreth, W. F. Bergfeld, D. V. Belsito, R. A. Hill, C. D. Klaassen, D. C. Liebler, J. G. Marks Jr, R. C. Shank, T. J. Slaga, P. W. Snyder and F. A. Andersen, *International journal of toxicology*, 2013, **32**, 5S-32S.
30. S. Moret, P. J. Dyson and G. Laurency, *Nat Commun*, 2014, **5**.
31. H. Hasse, I. Hahnenstein and G. Maurer, *AIChE Journal*, 1990, **36**, 1807-1814.
32. H. Hasse and G. Maurer, *Fluid Phase Equilib.*, 1991, **64**, 185-199.

Journal Name

33. G. Maurer, *AIChE Journal*, 1986, **32**, 932-948.
34. J. G. M. Winkelman, M. Ottens and A. A. C. M. Beenackers, *Chem. Eng. Sci.*, 2000, **55**, 2065-2071.
35. J. G. M. Winkelman, O. K. Voorwinde, M. Ottens, A. A. C. M. Beenackers and L. P. B. M. Janssen, *Chem. Eng. Sci.*, 2002, **57**, 4067-4076.
36. D. R. Kent Iv, S. L. Widicus, G. A. Blake and W. A. Goddard Iii, *J. Chem. Phys.*, 2003, **119**, 5117-5120.
37. M. Boudart, *Chem. Rev.*, 1995, **95**, 661-666.
38. V. S. Kislik, in *Liquid Membranes*, ed. V. S. Kislik, Elsevier, Amsterdam, 2010, pp. 17-71.
39. Z. N. Lou, Y. Xiong, J. J. Song, W. J. Shan, G. X. Han, Z. Q. Xing and Y. X. Kong, *Transactions of Nonferrous Metals Society of China (English Edition)*, 2010, **20**, s10-s14.
40. E. R. Kennedy, ed. U. S. D. o. H. a. H. Services, National Institute for Occupational Safety and Health, Ohio, 4 edn., 1994, ch. Formaldehyde: Method 3500.
41. Q. Li, P. Sritharathikhun and S. Motomizu, *Anal. Sci.*, 2007, **23**, 413-417.

Table of Contents text:

Discovery of a low temperature route to produce formaldehyde via catalytic hydrogenation of carbon monoxide in aqueous phase

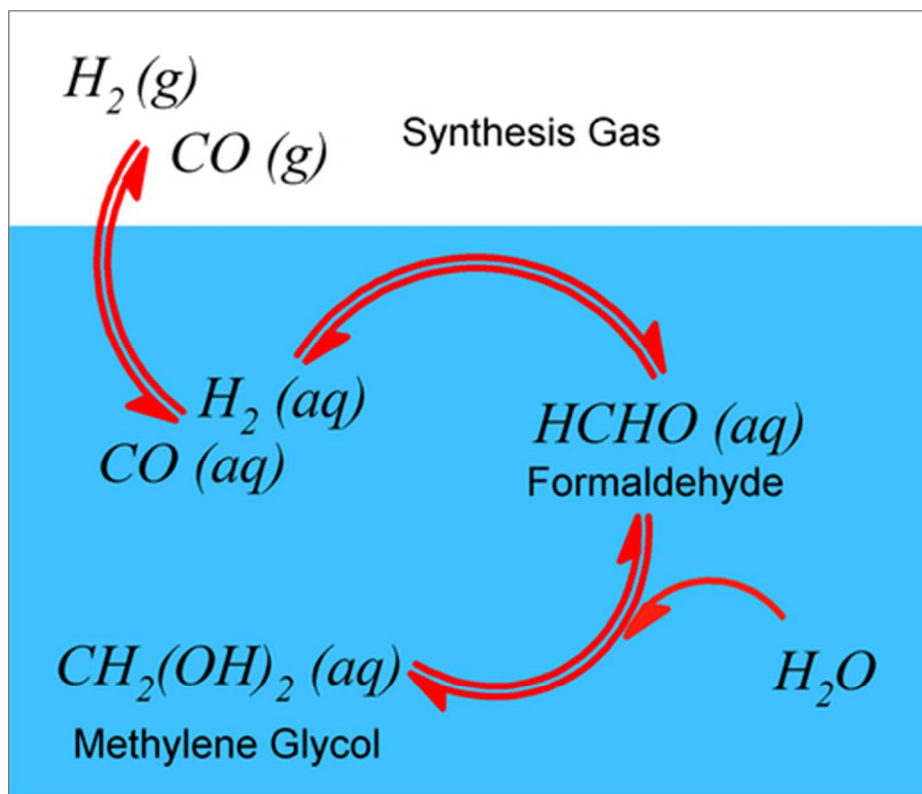


Table of Contents Graphic
39x33mm (300 x 300 DPI)